Bulk and Thin Film Ordering in Side-Chain Liquid-Crystalline/ Amorphous Diblock Copolymers: The Role of Chain Length

M. Al-Hussein* and W. H. de Jeu

FOM-Institute for Atomic and Molecular Physics, Kruislaan 407, 1098 SJ Amsterdam, The Netherlands

L. Vranichar, S. Pispas, and N. Hadjichristidis

Department of Chemistry, Athens University, Panepistimiopolis Zografou, 15771 Athens, Greece

T. Itoh and J. Watanabe

Department of Organic and Polymeric Materials, Tokyo Institute of Technology, Ookayama, Meguro-ku, Tokyo 152-8552, Japan

Received May 9, 2004; Revised Manuscript Received June 17, 2004

ABSTRACT: The ordering of a series of side-chain liquid-crystalline/amorphous diblock copolymers with different molecular weights, compositions, and polydispersities is reported. The diblock copolymers comprise polystyrene and poly(methacrylate) bearing methoxy biphenyl mesogenic groups. All samples show a lamellar morphology regardless of their molecular weights, compositions, and polydispersities. Apart from the low-molecular-weight sample, a smectic phase is observed at elevated temperatures. At room temperature, the mesogenic groups partially crystallize. For the sample with the lowest molecular weight the crystalline layers are uncorrelated, and their melting induces the order-to-disorder transition. Samples with relatively long main chains exhibit a three-dimensional ordered crystalline structure with a finite correlation length along the layer normal. This correlation length is longer for the sample with the lowest polydispersity. The mesogenic layers are always perpendicular to the block interfaces. These results can be understood in terms of changes in the conformation of the main chain of the liquid-crystalline block with its length. In thin films, the lamellae orient parallel to the interfaces in an asymmetric fashion with PS at the air interface. At the substrate a thin parallel mesogenic layer is induced. However, this parallel orientation does not propagate into the film interior, and the mesogenic crystalline layers retain their preferred perpendicular orientation with respect to the block lamellae.

1. Introduction

Side-chain liquid-crystalline diblock copolymers (SCLC-BCs) are synthesized by coupling a polymer with mesogenic side groups to a conformationally isotropic polymer.[1,2] This allows the combination of two self-organizing mechanisms in a single molecular system, driven by liquid-crystalline ordering of the mesogens and by the interblock incompatibility (microphase separation). Side-chain liquid-crystalline homopolymers can self-organize on length scales of 0.5 to a few nanometers in several phases. These range from a nematic phase with orientational order only, via smectic phases with low-dimensional ordering due to additional layering, to three-dimensionally ordered crystalline structures.[3] Meanwhile, the microphase separation phenomenon of diblock copolymers leads to the formation of well-defined periodic microdomains of controlled morphology (e.g., spheres, cylinders, bicontinuous structures, and lamellae) on a larger length scale (10−100 nm).[4,5] Therefore, the presence of the two ordering mechanisms in one system offers the possibility for simultaneously creating ordered structures at length scales in the range 0.5−100 nm. This is a key size for emerging technologies, and therefore SCLC-BCs hold the potential of creating new tailored materials with novel properties.[6]

In side-chain liquid-crystalline homopolymers, the liquid-crystalline order is determined by the interplay between the tendency of the main chains to form a random coil conformation and the tendency of the mesogenic groups to form ordered smectic layers. In SCLC-BCs, however, the LC block is constrained by its coupling to the isotropic block. The resulting confinement of the ordering of the LC block into discrete microdomains introduces further parameters into play. Although the influence of fundamental parameters such as the type and size of the morphology has been discussed,[7−11] the effect of other SCLC-BC parameters is still far from clear. Thus, a detailed understanding of the LC block ordering process and the effect of the SCLC-BC parameters on this ordering is needed in order to design new molecularly ordered functional materials.

In this work, we have investigated the ordering of a series of SCLC-BCs with the chemical structure shown in Figure 1. The phase behavior of the corresponding LC homopolymers and serval symmetric SCLC-BCs has been reported by Watanabe and co-workers.[8,12] In contrast, the samples investigated in this study encompass a range of compositions, molecular weights, and molecular weight distributions (polydispersities). The results show that, apart from a low-molecular-weight sample, all diblock copolymers show a microphase separation at high temperatures and smectic layering within the LC block at lower temperatures. At room temperature, all samples form two-dimensional crystalline layers within the LC block of the lamellar microphase-separated domains. However, the correlation of these layers along the normal direction shows a dependence on the main-chain length and its polydispersity. The ordering of selected diblock copolymers in

10.1021/ma049093l CCC: $27.50
Published on Web 07/30/2004

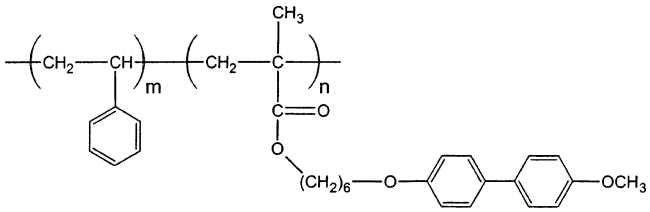

Figure 1. Molecular structure of the diblock copolymers.

Table 1. Characteristics of the Samples Used in This Study

sample	M_w	M_w/M_n	ϕ_{PS}	DP of LC block[a]	T_m (°C)	T_{iso} (°C)	morphology	L (nm)
A	9 900	1.25	0.80	6	93		lamellar	17.5
B	14 700	1.22	0.56	19	98	128	lamellar	19.0
C	18 800	1.22	0.44	30	98	128	lamellar	21.0
D	25 300	1.14	0.61	33	98	128	lamellar	25.2

[a] Weight-average value.

thin films was investigated using a combination of X-ray reflectivity (XR), atomic force microscopy (AFM), and grazing incidence X-ray scattering (GIXS). The results revealed a predominantly "bookshelf" structure, whereby the block lamellae and the mesogenic crystalline layers orient parallel and perpendicular to the substrate, respectively, in addition to a thin parallel mesogenic layer adjacent to the substrate.

2. Experimental Section

2.1. Samples. A series of diblock copolymers with different molecular weights and compositions were synthesized by living anionic polymerization following the procedure reported by Yamada et al.[8] Their characteristics are listed in Table 1. The liquid-crystalline block is poly(6-[4-(4-methoxyphenyl) phenoxy]hexyl methacrylate) (PMPPHM) while the amorphous block is polystyrene (PS) (Figure 1). Samples A, B, and C have comparable polydispersities but different molecular weights while sample D has a relatively higher molecular weight and lower polydispersity. The weight-average molecular weight of the polystyrene block was 7800 for the first three samples, but for the fourth one it was 13 000. This resulted in different average main-chain lengths of the LC block in the different samples. Sample A has the shortest main chain while samples C and D have a comparable size of the LC block. All samples were investigated after melting at 180 °C for 10 min; subsequently, they were cooled slowly to room temperature.

2.2. Small- and Wide-Angle X-ray Scattering. Small- and wide-angle X-ray scattering (SAXS and WAXS) measurements were conducted using an in-house setup with a rotating anode X-ray generator (Rigaku RU-H300) operating at 18 kW. By employing two parabolic multilayer mirrors (Bruker, Karlsruhe), a highly parallel beam of a monochromatic Cu Kα radiation ($\lambda = 0.154$ nm) with a divergence of 0.012° was obtained. A Linkam CSS450 shear cell was used as a temperature-controlled sample stage. The SAXS patterns were recorded with a Bruker Hi-Star area detector at two sample-to-detector distances: 0.37 and 1.03 m. The two-dimensional scattering patterns were radially integrated, corrected for the background, and then displayed as one-dimensional plots of the intensity as a function of $q = (4\pi/\lambda) \sin \theta$, the modulus of the scattering vector **q**, where θ is half the scattering angle. The WAXS curves were recorder using a linear position-sensitive detector (PSD-50M, Braun).

2.3. Atomic Force Microscopy. Thin films were spin-coated from toluene solution onto a Si wafer. Their surface morphology was investigated by atomic force microscopy (AFM) at room temperature using a Solver SFM, NT-MDT (Zelenograd, Moscow), in the tapping mode. A standard cantilever with a resonant frequency about 300 kHz and a silicon tip with a curvature radius of 10 nm was used.

2.4. X-ray Reflectivity. For X-ray reflectivity measurements the Cu Kα radiation was collimated in the scattering plane only by a W/B_4C graded parabolic multilayer mirror. The samples were mounted vertically at the center of a two-circle goniometer and investigated under specular reflection conditions. Additional presample and predetector slits resulted in an overall resolution of $\Delta q_z = 0.03$ nm^{-1}.

2.5. Grazing Incidence X-ray Scattering. The experiments were carried out on beamline BW2 (HASYLAB, Hamburg) at 10 keV ($\lambda = 0.124$ nm). For the geometry used, the incident, exit, and out-of-plane angles are defined as α_1, α_2, and ψ, respectively. The scattering vector is given by $q_x = (2\pi/\lambda)(\cos \psi \cos \alpha_2 - \cos \alpha_1)$, $q_y = (2\pi/\lambda)(\sin \psi \cos \alpha_2)$, and $q_z = (2\pi/\lambda)(\sin \alpha_1 + \sin \alpha_2)$. To maximize the measured signal from the full film, α_1 was set at 0.167° in between the critical angle for total reflection of the diblock polymer film and that of the Si substrate. The slits used resulted in an overall resolution in the sample plane of $\Delta\psi = 0.144°$. The scattered intensity was recorded at different out-of-plane angles using a scintillation detector.

3. Results

3.1. Bulk. Figures 2 and 3 show typical SAXS and WAXS curves of the four samples taken for the different phases of the LC block, respectively. The SAXS curves provide a clear evidence for microphase-separated structures for samples B, C, and D at all temperatures and for sample A only at temperatures lower than 93 °C. The sharp peaks at $q = 0.25$, 0.30, 0.33, and 0.36 nm^{-1} for samples D, C, B, and A, respectively, with corresponding higher-order peaks, indicate a lamellar morphology in all cases. The resulting lamellar periods are listed in Table 1. The WAXS curves of Figure 3 indicate a partially crystalline nature of all samples at room temperature. Each of the curves comprises two crystalline reflections superimposed on a broad amorphous halo. Watanabe and co-workers investigated the crystalline structure of similar diblock copolymers in detail.[8] They found that the crystalline reflections can be indexed by an orthorhombic unit cell with $a = 0.800$ nm, $b = 0.541$ nm, and $c = 2.580$ nm, indicating a crystalline-E phase (Cr-E). Because of the limited measured q range of Figure 3, only two crystalline reflections are observed. The positions of these two reflections coincide with those measured by Watanabe and co-workers. Therefore, it can be concluded that for all samples the neighboring biphenyl mesogenic groups are crystallized into a two-dimensional lattice within individual layers.

For sample A, the crystalline WAXS reflections disappear at temperatures around 93 °C, leaving only the amorphous halo behind. This indicates melting of its mesogenic crystalline layers. At the same temperature, changes occur in the SAXS curve: the higher reflection orders disappear, and a significant broadening of the first-order peak takes place. Evidently, the lamellar microphase-separated structure gets lost, indicating that melting of the crystalline layers induces the order-to-disorder transition in this sample.

For the other three samples, B, C, and D, the crystalline reflections disappear at a slightly higher temperature of 98 °C. Furthermore, complementary polarized light microscopy reveals birefringent features at temperatures above their melting points, indicative of a LC order. The birefringence persists until they become isotropic above 128 °C. Table 1 summarizes the morphological characteristics, the melting temperature, T_m, and the isotropization temperature of the LC block, T_{iso}, for all samples.

Figure 4 shows SAXS curves obtained with a shorter sample-to-detector distance (larger q range) to probe the

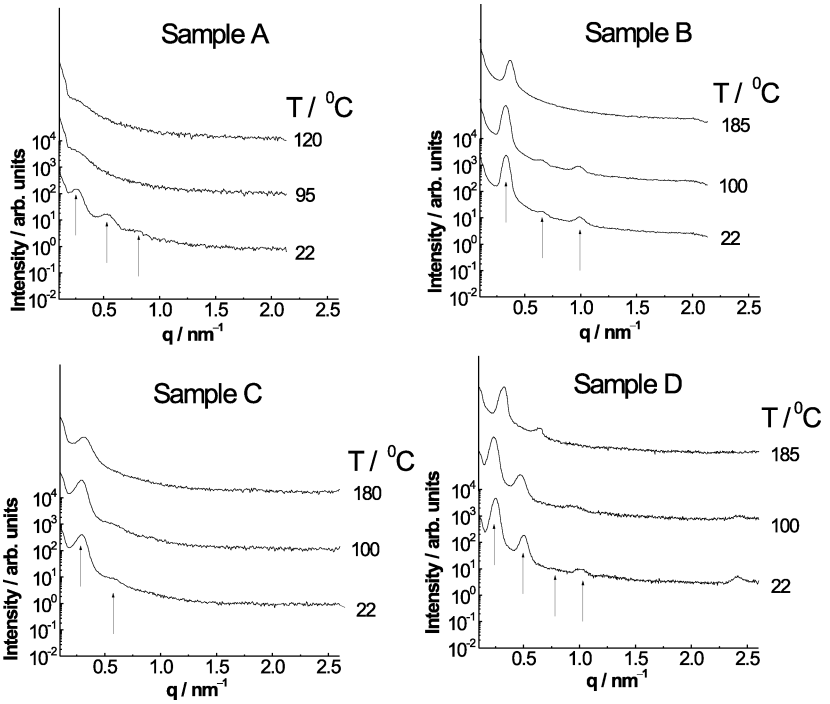

Figure 2. SAXS curves obtained at the indicated temperatures (sample-to-detector distance 1.03 m; arrows indicate the lamellar reflections). Curves are shifted vertically for clarity.

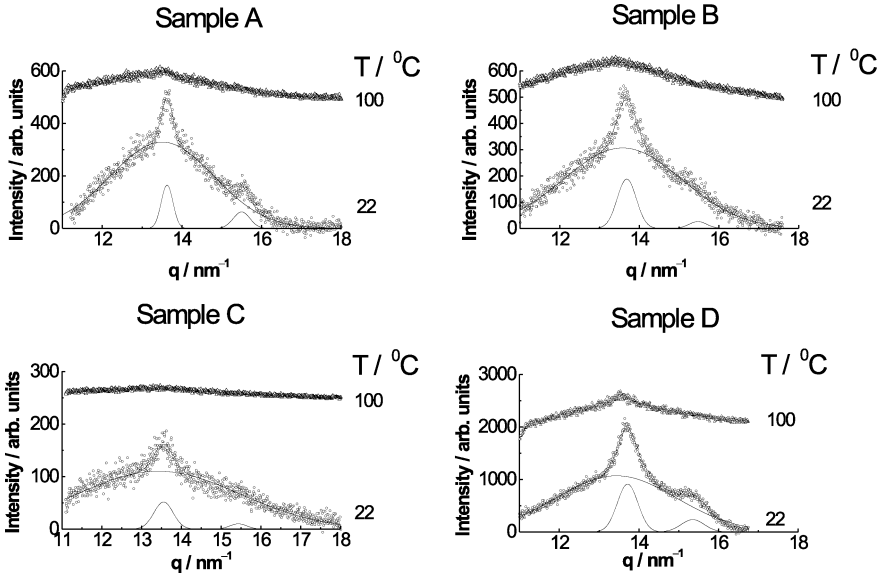

Figure 3. WAXS curves obtained at the indicated temperatures.

layering for the different phases of the LC block in samples B, C, and D. Sample D, with the lowest polydispersity and relatively long main chain, shows two orders of equally spaced sharp reflections in both the crystalline and smectic phases of the LC block, albeit the low intensity in the smectic phase. As the crystallinity of the layers disappears above 98 °C, the high-temperature LC phase can be identified as smectic-A (Sm-A). It is noteworthy that the first-order reflection exhibits a lower intensity than the second-order one. The other two samples, B and C, with relatively high polydispersities, show almost identical behavior, whereby broad and weak peaks are observed at the same q values as for sample D. To determine the relative orientation of the crystalline layers with respect to the block copolymer lamellar morphology, an oriented fiber specimen was prepared by pulling from the isotropic melt. Figure 5 shows the SAXS pattern of an oriented fibre specimen prepared from sample D at room temperature. As it can be seen, the lamellar reflections and the mesogenic crystalline layers reflections are orthogonal to each other. Therefore, it can be concluded that the mesogenic crystalline layers are perpendicular to the block lamellar morphology.

3.2. Thin Films. The nanostructures of thin films prepared from samples B, C, and D were characterized using a combination of X-ray reflectivity (XR), atomic force microscopy (AFM), and grazing incidence X-ray scattering (GIXS). Essentially, they all show a similar behavior, and therefore we only present the results of sample D in the following. Shown in Figure 6 are rocking curves of a film annealed at 160 °C for 24 h. In a rocking scan, the sample and the detector are placed at the specular position first, i.e., $\alpha_1 = \alpha_2$; then the

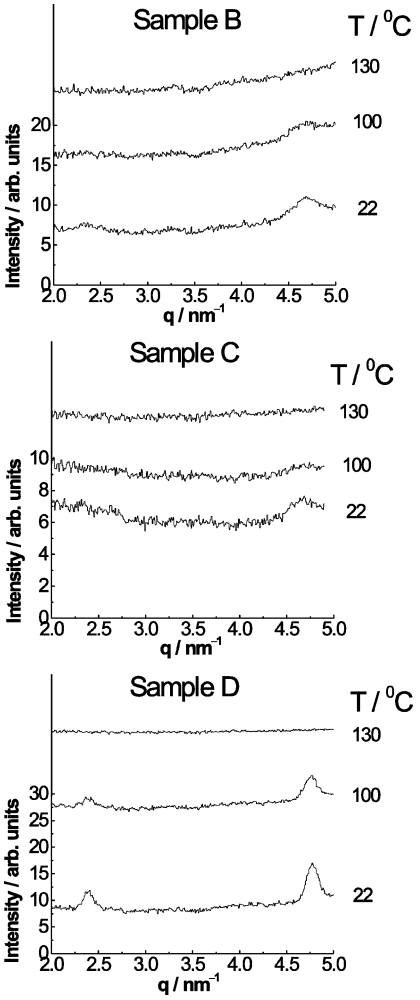

Figure 4. SAXS curves obtained at the indicated temperatures (sample-to-detector distance 0.37 m).

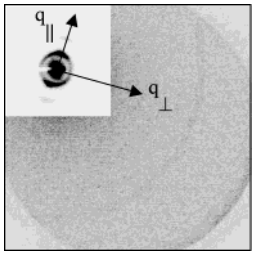

Figure 5. SAXS diffraction pattern of oriented fibre specimen of sample D at room temperature.

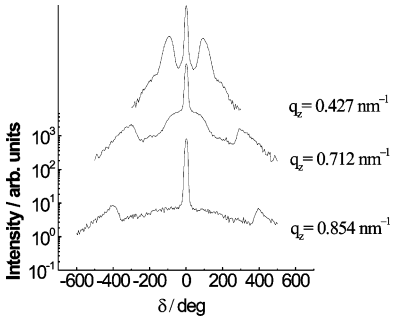

Figure 6. Rocking curves of an annealed film of sample D at the indicated q_z values.

sample is rocked over $\omega = \alpha_1 - \alpha_2$ while keeping $\alpha_1 + \alpha_2$ fixed. The mosaicity of the film, i.e., the fwhm of the specular reflection (central maxima of Figure 6), is

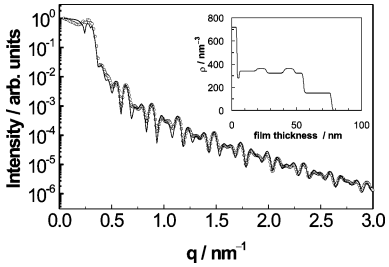

Figure 7. X-ray reflectivity curve of an annealed film of sample D at room temperature (open circles); solid line is calculated using the electron density profile in the inset.

Table 2. Best-Fit Parameters Obtained from Fitting the Reflectivity Curve

layer	t (nm)	σ (nm)	ρ (nm $^{-3}$)
Si_2	∞	0.5 ± 0.01	719
SiO_2	3.6 ± 0.03	0.24 ± 0.02	719
1	1.84 ± 0.02	0.30 ± 0.02	284 ± 5
2	13.69 ± 0.35	0.81 ± 0.03	347 ± 7
3	7.80 ± 0.06	0.70 ± 0.01	361
4	13.69 ± 0.35	0.81 ± 0.03	323
5	7.80 ± 0.07	0.69 ± 0.02	361
6	7.31 ± 0.09	0.60 ± 0.02	323
7	21.62 ± 0.43	0.62 ± 0.02	151 ± 3

typically 0.012°. The two peaks at $\omega = \pm\alpha_c$ are the so-called Yoneda peaks[13] and are due to dynamic effects. Figure 7 shows a typical XR reflectivity curve of the same film. The oscillations result from interference of the X-ray scattered from the air−film and the film−substrate interfaces (Kiessig fringes) and provide information about the total film thickness. The modulation in the amplitude of the fringes with a beat frequency indicates the presence of different thicknesses (steps) at the film surface.[14] No Bragg peaks from the mesogenic crystalline layers are observed in the XR curve. To obtain more quantitative information about the structure perpendicular to the substrate of the annealed film, its XR curve was fitted using an iterative matrix solution of the Fresnel equations.[15] The sample was represented by a succession of layers; each has its own electron density, ρ, thickness, t, and a Gaussian interfacial roughness, σ. The best fit of the XR curve was achieved by a succession of seven layers with a total film thickness of 73 ± 2 nm. The calculated reflectivity curve is in a good agreement with the measured one over the whole q range investigated (see Figure 7). The parameters used for the fitting or extracted from it are listed in Table 2. More details of the model are given in section 4.2.

AFM images of annealed film surfaces are rather smooth. In addition, holes with different lateral sizes are observed on the surface. The average depth of the holes is about 22 nm, approximately a single block period. Such a smooth terraced morphology is typical for the confined situation of diblock copolymers with their lamellae oriented parallel to the substrate,[16,17] which restricts the film thickness to $(n + {}^1/_2)L$ in the case of asymmetric wetting.

The XR curve shows no evidence indicating that the mesogenic crystalline layers are oriented parallel to the substrate. In the bulk state, the oriented sample indicated that they orient perpendicular to the block copolymer interfaces. If the bulk orientation remains the same in thin films, the mesogenic lamellae will be oriented perpendicular to the substrate. However, this is not always the case; the mesogenic groups might

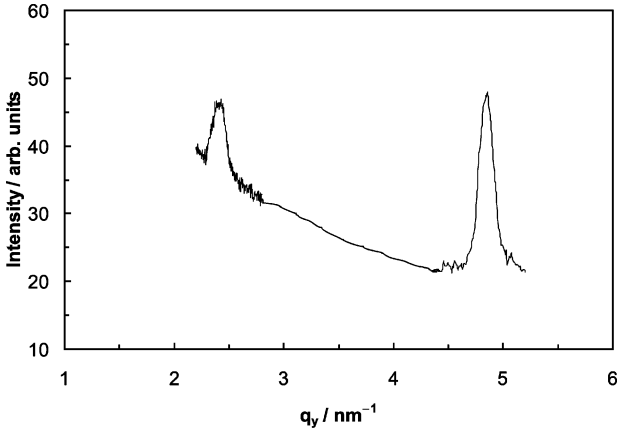

Figure 8. Grazing incidence X-ray scattering curve of an annealed film of sample D at room temperature showing first and second reflections.

change their orientation in thin films if they exhibit a strong anchoring tendency onto either the substrate or the free surface.[18] To probe any possible ordering of the mesogenic layers in the film plane, the annealed film was studied by GIXS. The intensity profile parallel to the film surface is shown in Figure 8. Two orders of equally spaced reflections characteristic of the correlation of the mesogenic crystalline layers along their normal can be clearly seen.

4. Discussion

4.1. Bulk. 4.1.1. Low-Molecular-Weight Sample A. At room temperature, sample A shows no discernible peaks in the q range where the other samples show layering. This indicates the absence of any correlation between its crystalline layers along their normals. This is probably not surprising considering the small size of its LC block (six mesogenic units), which is comparable to the length of the mesogenic group. In fact, measurements performed on narrow fractions of SCLC homopolymers showed that the number of mesogenic groups has to be more than 12 in order to form a smectic phase (see for example ref 19).

A lamellar morphology is not expected for sample A on the basis of its composition.[4] It has 80% PS, and according to the phase diagram of an isotropic−isotropic diblock copolymer, the expected morphology should be hexagonally packed cylinders of the LC phase in a PS matrix, rather than lamellar. We attribute this extension in the stability range of the lamellar phase to the interplay between microphase separation and crystallization of the mesogens in layers. Because of the low molecular weight of this copolymer, its order-to-disorder transition temperature is low, which is determined by χN, where χ is the Flory−Huggins parameter and N is the total degree of polymerization.[5] Upon cooling from the isotropic melt, the order-to-disorder transition will not happen unless the LC crystallization takes place. Crystallization of the mesogens results in a substantial increase in χ and in turn dominates the phase separation process, leading to the formation of a lamellar morphology even at such a low LC volume fraction (0.20).

4.1.2. Molecular Weight Dependence. The results show that in all samples the mesogenic side groups form crystalline layers in combination with lamellar microphase-separated domains at low temperatures, regardless of their molecular weights, compositions, and

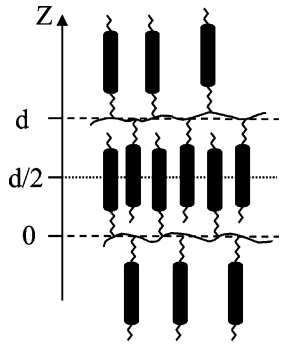

Figure 9. Schematic representation of the LC phase structure.

polydispersities. The samples with a large molecular weight exhibit in addition at higher temperatures a Sm-A LC ordering. Evidently, the small size of the LC block of sample A prevents the formation of a Sm-A phase.[8] The first-order peak at $q = 2.44$ nm^{-1} corresponds to a layer spacing of 2.57 nm. The calculated fully extended length of the side group is about 2.2 nm, which indicates an interdigitated packing of the mesogenic groups. Moreover, the second-order layer reflection is much stronger than the first-order one, indicating an additional plane of symmetry in the electron density profile. This can occur when the electron densities in both the main chain layer and the mesogenic layer are almost equal. In that case an apparent spacing of half the length of the mesogenic units is induced (see Figure 9), making the "second order" a new fundamental spacing.

According to Figure 4, the differences in the behavior of samples B, C, and D are not significant. In all cases correlation exists between the crystalline layers of the low-temperature Cr-E phase. However, the narrower peaks in sample D indicate a larger correlation length $\xi \simeq 35$ nm along the layer normal. For samples B and C it is only about 21 nm. As the latter samples have relatively high polydispersities, we tentatively associate the narrow peaks of sample D with its lower polydispersity.

4.1.3. Influence of Polydispersity. As mentioned above, a large polydispersity seems to restrict the long-range order of the mesogenic layers along their normal direction. In principle, two causes can contribute to the broadening of the layer peak: first, a finite size of layer domains along the layer normal; second, an intrinsic finite correlation range between the layers along their normal. It is not easy to distinguish between the effects of the two causes, and it may well be that the latter gives rise to the former.

Though the exact nature of a possible correlation between polydispersity and ordering of the mesogenic layers along their normal is not evident, we will speculate about a possible explanation. A finite correlation range may result from defects in the packing of the mesogenic groups due to the distortion introduced by the polymer main chain. According to small-angle neutron scattering of LC homopolymers with methacrylate main chains, long main chains are more strongly confined between the mesogenic layers than shorter ones.[20,21] Hence, the short main chains in samples with a relatively high polydispersity may act as defects limiting the number of correlated mesogenic layers. Therefore, it is conceivable that also in our case short main chains are less confined between the mesogenic

layers which facilitates hopping between the layers with a lower energy penalty. This can be expected to reduce the block size along the layer normal and distort the interlayer packing.

Though the difference in polydispersity between samples C and D provides a natural explanation of the observed differences in correlation length between the mesogenic layers, one should realize that for sample D the size of the PS block is appreciably larger than for sample C. This leads to less stretching of the LC block of sample D compared to C, even though the LC blocks are of a similar size in both samples. Though it is not clear to us how stretching along the backbone could affect the correlation normal to this direction, some precaution regarding our explanation seems appropriate.

4.2. Thin Films. The morphology and orientation of thin films of diblock copolymers are influenced by the interactions of both blocks with the top and bottom interfaces.[14,22] If one of the blocks is a side-chain liquid crystalline polymer, the specific anchoring interaction of its mesogens with either of the interfaces can play an additional role. The AFM results indicate that the diblock copolymers exhibit typical parallel block lamellae in thin films. More insights regarding the structure along the film normal can be gained from the fitting results of the XR curve. The best fit was achieved using a density profile comprised of seven layers. The electron densities used for layers 3−6 were based on the known bulk densities of PS and PMPPHM. The densities of layers 1 (adjacent to the substrate), 2, and 7 (the top layer) together with the thickness and roughness of all layers were extracted from the fitting. The middle periodic layers (2, 3, 4, and 5) make up two lamellar periods with a period $L = 21.5 \pm 0.4$ nm, which is smaller than the bulk period (25.2 nm). The extracted thicknesses of the PS and the LC sublayers are 13.7 and 7.8 nm, respectively. This in good agreement with the expected thicknesses given the volume fraction of PS ($\phi_{PS} = 0.61$) and $L = 21.5$ nm, namely 13.1 and 8.4 nm, respectively. Layer 6 has the same density as PS, and its thickness is approximately half the thickness of the PS sublayer. Meanwhile, the thickness of the top layer, layer 7, is 21.6 nm, again approximately a complete lamellar period. Its low density can be attributed to the holes that form at the surface, which effectively reduce the electron density by an amount commensurate with their surface coverage. Note here that the lamellar period extracted from the fitting is very close to the average height of the holes at the surface as revealed by AFM. The fact that the density of layer 6, just below the top layer of thickness L, is identical to the PS sublayer proves that the film exhibits an asymmetric wetting with the PS block at the air surface and the PMPPHM block at the substrate. However, the thickness of layer 1 (1.8 nm) is very much smaller than half the PMPPHM sublayer (3.9 nm, as expected for a standard asymmetric wetting). Moreover, its density is also lower than either one of the sublayers of the two blocks. Interestingly, the thickness of this layer is close to the size of the mesogenic groups in its fully extended form (2.2 nm). These observations can be explained by assuming that the mesogens exhibit a homeotropic anchoring onto the substrate. This induces a thin parallel mesogenic layer adjacent to the substrate. Such a layer is made of mesogens that point mainly downward with respect to the main chain only, and therefore its density is expected to be lower than the interdigitated crystalline layers of the bulk state. This implies that the remaining mesogens that point upward with respect to the main chain are forced to intermix with the adjacent PS block. The fact that the extracted density of layer 2, which is adjacent to layer 1, is higher than that of the PS block supports this proposition.

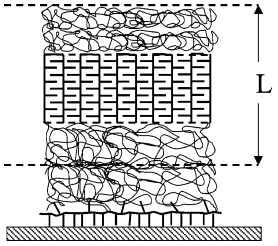

Figure 10. A proposed model for the thin film structure.

The GIXS results (Figure 8) show two orders of Bragg peaks characteristic of the mesogenic crystalline layers in the film plane. This indicates that a large proportion of the layers is oriented perpendicular to the substrate. Moreover, the XR curve shows no Bragg peaks that correspond to a parallel orientation of the mesogenic crystalline layers. These observations suggest that although a thin mesogen layer forms parallel to the lamellar block domains at the substrate, this parallel orientation does not propagate through the film. Figure 10 shows the model proposed for the film structure based on these observations. The PMPPHM block wets the silicon substrate with a single monolayer, and the PS block wets the air surface. The mesogens anchor homeotropically at the substrate in order to minimize the interfacial free energy. This results in unfavorable mixing between some of the mesogens and the PS block and a potential frustration due to incommensurability between the block lamellar domain period, the mesogenic spacing, and the film thickness. Therefore, as the influence of the anchoring interaction subsides with increasing distance from the silicon substrate, the PMPPHM block retains its preferred perpendicular orientation through the entire film. Sentenac et al. reported a similar parallel orientation at the substrate that was maintained throughout the entire film for a different set of SCLC-BCs.[18] However, in their samples the main chain of the LC block was similar to the amorphous polymer with the interaction parameter being virtually zero. Then the microphase separation stems mainly from the interaction between the polymer (both backbone and amorphous block) and the mesogens. In our case this is very different, and therefore a perpendicular orientation is preferred in order to minimize the contact area between backbone chain and the amorphous block.

5. Conclusions

Ordering of a series of side-chain liquid-crystalline diblock copolymers with a range of molecular weights, polydispersities, and compositions has been investigated. In all samples, the mesogenic side groups form at room temperature two-dimensional crystalline layers within lamellar microphase-separated domains. However, the correlation of these layers along the normal direction shows a dependence on the main chain length and its polydispersity. The sample with short main chains show no correlation between the crystalline layers. In this case the melting of the mesogens causes

an order−disorder transition of the blocks. The samples with relatively long main chains exhibit a three-dimensional crystalline structure, crystal-E. For these samples an increase in the polydispersity leads to a reduced correlation between the crystalline layers. This is attributed to an increased presence of short main chains that are less confined between the mesogenic layers, facilitating hopping between adjacent layers. This distorts the interlayer packing which in turn limits the range of correlation between the crystalline layers along their normals. In thin films the block lamellae are parallel to the substrate, while in the film interior the mesogenic layers retain their preferred perpendicular orientation with respect to the block lamellar interfaces. However, the preferential anchoring of the mesogens onto a Si substrate results in a thin parallel mesogenic layer at the substrate only.

Acknowledgment. The authors thank B. I. Ostrovskii for helpful discussions. This work is part of the research program of the "Stichting voor Fundamenteel Onderzoek der Materie (FOM)", which is financially supported by the "Nederlandse Organisatie voor Wetenschappelijk Onderzoek (NWO)". This work was financially supported by the EU-network POLYNANO under Contract HPRN-CT-1999-00151.

References and Notes

(1) Walther, M.; Finkelmann, H. *Prog. Polym. Sci.* **1996**, *21*, 951.
(2) Poser, S.; Fischer, H.; Arnold, M. *Prog. Polym. Sci.* **1998**, *23*, 1337.
(3) Shibaev, V. P., Lam, L., Eds.; *Liquid Crystalline and Mesomorphic Polymers*; Springer-Verlag: New York, 1994.
(4) Bates, F. M.; Fredrickson, G. H. *Annu. Rev. Phys. Chem.* **1990**, *41*, 525.
(5) Hamley, I. W. *The Physics of Block Copolymers*; Oxford: New York, 1998.
(6) Mao, G.; Ober, C. K. *Acta Polym.* **1997**, *48*, 405.
(7) Fischer, H.; Poser, S.; Arnold, M.; Frank, W. *Macromolecules* **1994**, *27*, 7133.
(8) Yamada, M.; Iguchi, T.; Hirao, A.; Nakahama, S.; Watanabe, J. *Macromolecules* **1995**, *28*, 50.
(9) Sänger, J.; Gronski, W.; Maas, S.; Stühn, B.; Heck, B. *Macromolecules* **1997**, *30*, 6783.
(10) Mao, G.; Wang, J.; Clingman, S. R.; Ober, C. K.; Chen, J. T.; Thomas, E. L. *Macromolecules* **1997**, *30*, 2556.
(11) Anthamatten, M.; Hammond, P. T. *Macromolecules* **1999**, *32*, 8066.
(12) Yamada, M.; Iguchi, T.; Hirao, A.; Nakahama, S.; Watanabe, J. *Polym. J.* **1998**, *30*, 23.
(13) Yoneda, Y. *Phys. Rev. Lett.* **1963**, *131*, 2010.
(14) Russell, T. P. *Mater. Sci. Rep.* **1990**, *5*, 171.
(15) Tolan, M. *X-ray Scattering from Soft Matter Thin Films*; Springer: Berlin, 1999.
(16) Coulon, G.; Ausserre, D.; Russell, T. P. *J. Phys. (Paris)* **1990**, *51*, 777.
(17) Maaloum, M.; Ausserre, D.; Chatenay, D.; Coulon, G.; Gallot, Y. *Phys. Rev. Lett.* **1992**, *68*, 1575.
(18) Sentenac, D.; Demirel, A. L.; Lub, J.; de Jeu, W. H. *Macromolecules* **1999**, *32*, 3235.
(19) Boiko, N.; Shibaev, V. P.; Ostrovskii, B.; Sulyanov, S.; Wolff, D.; Springer, J. *Macromol. Chem. Phys.* **2001**, *202*, 297.
(20) Moussa, F.; Cotton, J. P.; Hardouin, F.; Keller, P.; Lambert, M.; Pepy, G.; Mauzac, M.; Richards, H. *J. Phys. (Paris)* **1987**, *48*, 1079.
(21) Richardson, R. M.; Barmatov, E. B.; Whirehouse, I. J.; Shibaev, V. P.; Yongjie, T.; Godinho, M. H. F. *Mol. Cryst. Liq. Cryst.* **1999**, *330*, 285.
(22) Fasolka, M. J.; Mayes, A. M. *Annu. Rev. Mater. Res.* **2001**, *31*, 323.

MA049093L